

# 1 Fault zone permeability structure evolution in basalts

2 **Richard J. Walker<sup>1,2</sup>, Robert E. Holdsworth<sup>2</sup>, Peter J. Armitage<sup>3</sup>, and Daniel R. Faulkner<sup>3</sup>**

3 *<sup>1</sup>School of Earth and Ocean Science, Cardiff University, Park Place, CF10 3AT, UK*

4 *<sup>2</sup>Department of Earth Sciences, Durham University, Science Labs, Durham, DH1 3LE, UK*

5 *<sup>3</sup>Rock Deformation Laboratory, University of Liverpool, Liverpool, L69, 3BX, UK*

## 6 **ABSTRACT**

7       A combination of field, microstructural and experimental static permeability  
8 characterization is used to determine fault permeability structure evolution in upper crustal  
9 basalt-hosted fault zones in the Faroe Islands. The faults comprise lower strain fracture networks,  
10 to higher strain breccias that form tabular volumes around a principal slip zone hosting gouge or  
11 cataclasite. Samples representative of these fault zone components are used for static  
12 experimental permeability measurement. Results indicate that within the appropriate effective  
13 pressure (depth) range (10–90 MPa: ~0.3 to ~3.0 km), basalt-hosted faults evolve from low strain  
14 (< 1m displacement), relatively low-permeability (<10–17 m<sup>2</sup>) structures, to high strain (≥ 1m  
15 displacement), relatively high-permeability (>10–17 m<sup>2</sup>) structures. Sample analyses reveal that  
16 static permeability is controlled by the development of: a) fault-parallel clay alteration  
17 (decreasing permeability); and b) porous zeolite vein connectivity due to hydrofracture  
18 (increasing permeability). Fault-parallel permeability is increased relative to the host rock, while  
19 fault-normal permeability is low throughout fault rock evolution. This configuration will tend to  
20 promote across-fault compartmentalization and along-fault fluid flow, facilitating migration  
21 between relatively high-permeability horizons (e.g. vesicular flow unit tops and siliciclastic  
22 horizons), bypassing the bulk of the stratigraphy.

## 23 **INTRODUCTION**

24           The need to understand subsurface fluid flow and sealing potential in basaltic sequences  
25 is becoming increasingly important with the rising economic significance of intra- and sub-  
26 volcanic hydrocarbon plays (Schutter, 2003), conventional and enhanced geothermal systems,  
27 and the growing need to find suitable sites for geological carbon sequestration or storage  
28 (Hawkins, 2004; Oelkers and Cole, 2008). The efficacy of geological CO<sub>2</sub> storage is dependent  
29 on the retention time, the dynamic reservoir stability (the risk of leakage), and/or the mineral  
30 storage potential of the host rock (Gislason et al., 2010). Sealing potential in basaltic sequences  
31 is also important to intra- and sub-basaltic hydrocarbon plays, particularly in passive margin  
32 continental basins that are active targets for hydrocarbon exploration. In volcanic geothermal  
33 systems, the methods used for geothermal exploration and resource development are highly  
34 dependent on whether heat is lost by convection or conduction, and so fault permeability is  
35 critically important.

36           Faults are a key component in the sealing potential of any subsurface storage system, yet  
37 little is known about the hydraulic structure of basalt-hosted faults. Here we focus on part of the  
38 European North Atlantic margin (Fig. 1A; *Appendix 1*), which is covered by variable thicknesses  
39 of basaltic lavas and volcanoclastic rocks related to the North Atlantic Igneous Province. Several  
40 recent onshore and offshore studies in the Faroe-Shetland Basin (e.g., Ellis et al., 2009; Moy and  
41 Imber 2009; Walker et al. 2011a,b) have shown that faults cut part, or all of the Palaeocene lava  
42 sequence together with the rocks in the underlying sedimentary basins. It is important, therefore,  
43 to determine the permeability characteristics of such lava-hosted faults since they will likely  
44 influence fluid flow in the sub-surface.

45           Fluid flow in upper-crustal brittle fault zones is dependent on the permeability of the fault  
46 rock assemblage and its architecture (e.g., Faulkner and Rutter, 2001). Models for clastic

47 sedimentary sequences and crystalline basement rocks typically refer to a low-permeability *fault*  
48 *core* surrounded by a higher-permeability *damage zone*, relative to the intermediate permeability  
49 of the undeformed host rock (e.g., Caine et al., 1996; Evans et al., 1997). In this paper, we detail  
50 the permeability structure of basalt-hosted fault zones using examples of widely distributed  
51 brittle fracturing in the Faroe Island Basalt Group (FIBG) on the NE Atlantic Margin. This study  
52 uses experimental permeability measurements to quantify fault zone static permeability structure  
53 in basalts. Qualitative field- and microstructural characterization of the same fault rock  
54 assemblages are used to rationalize measured permeability, and to infer dynamic permeability  
55 associated with fault events. The results indicate that permeability during faulting is important in  
56 fluid migration, and, at stages in fault evolution low-strain zones can act as a barrier to fluid  
57 flow, whereas high-strain zones act as conduits.

## 58 **FAULT ZONE ARCHITECTURE**

59         Fault zones in the Faroe Islands cut volcanic and volcanoclastic strata of the Palaeocene-  
60 age Faroe Islands Basalt Group (FIBG: 59–56 Ma; Passey and Jolley, 2009), and are  
61 representative of faulting at depths between 1 and 3 km (Walker et al., 2012), formed before,  
62 during and immediately after North Atlantic break-up in the early Eocene (Walker et al., 2011a).  
63 Basaltic host units display joints and microfractures formed during cooling, which range in  
64 length from <1 mm up to ~30 m (i.e., the thickness of the host unit). Fractures and joints of this  
65 type increase in density toward the top of lava units, and toward the margins of dykes. Fault-  
66 related damage represents an increase in fracture density, relative to the host lithology. Slip is  
67 accommodated on a surface or zone of cataclasite or gouge, defining the *principal slip surface* or  
68 *zone* (PSS or PSZ respectively: Figure 1A, D). These are contained within the *fault core*, which  
69 is defined here as the zone that accommodates the majority of shear displacement, and can be

70 characterized by mosaic and chaotic breccias (Fig. 1A, C) (breccia definitions following  
71 Woodcock et al., 2006). Surrounding the fault core is a zone of damage, which is characterized  
72 by crackle to mosaic breccias (Fig. 1A, B).

73 Calcite and zeolite mineralization are ubiquitous in syn-magmatic Faroe Islands fault  
74 zones, indicating that they acted as conduits for the passage of hydrous fluids. Early-formed  
75 veins are filled with zeolite that grows inwards from the fracture walls as hemiradial fibers,  
76 indicating mineral growth into fluid-filled cavities. In thicker veins (>1–2 mm thick), calcite is  
77 typically the dominant mineral fill. In most fault zones, zeolites are also observed lining the  
78 euhedral terminations of individual calcite crystals. Textural relationships suggest that zeolite  
79 and calcite mineralization were accompanied by the generation of authigenic clays at all stages  
80 of fault zone evolution (Walker et al., 2012).

## 81 **METHODS**

82 Host rock and fault zone assemblages were sampled in transects across representative  
83 fault zones in the Faroe Islands, to characterize fault zone heterogeneity. The experimental static  
84 permeability measurements detailed below have sample volumes on the scale of cubic  
85 centimeters. Since mesoscopic open fractures have not been sampled explicitly, measured  
86 permeabilities may only provide a lower bound to the bulk fault zone permeability. Cores were  
87 taken to measure fault-parallel and fault-normal permeability, but, in most cases, the fault-  
88 parallel samples broke along fractures and veins, and could not be loaded into the high pressure  
89 fluid-flow apparatus. Static permeability was measured experimentally under simulated  
90 subsurface reservoir pressures (0.3 to 3.0 km) using the Transient Pulse Decay (TPD) technique  
91 (Brace et al., 1968): a detailed methodology is provided by Armitage et al. (2011). Argon was  
92 used as the permeant, and all experiments were conducted at a maintained room temperature of

93 ~22°C. The resolution of the pressure measurements is  $\pm 0.3$  MPa, and permeability can be  
94 measured accurately within the range  $10^{-16}$  to  $10^{-23}$  m<sup>2</sup> using our set-up for the TPD technique.

## 95 **STATIC PERMEABILITY RESULTS**

96 The bulk permeability structure of a fault zone is a composite of the properties of the  
97 architectural elements and their spatial arrangement in three dimensions (e.g., Caine and Forster,  
98 1999). Permeability measurements of the key fault zone components provide an indication of in  
99 situ permeability. On the assumption that low-strain fault rock components represent early stages  
100 of high-strain zones, these data can be used to infer the evolution of static permeability through  
101 time.

102 Pressure cycling within the study range (i.e., 10–90 MPa effective pressure) was used  
103 here to close any stress-relief micro-fractures (see *Appendix 2* for details). Our data reveal that at  
104 a simulated depth of ~3 km (90 MPa), permeability spans over four orders of magnitude, ranging  
105 from  $1.32 \times 10^{-20}$  m<sup>2</sup> (L03; Fig. 2) to  $1.44 \times 10^{-16}$  m<sup>2</sup> (L05; Fig. 2). For samples with fault-parallel  
106 ( $k_V$ ) and fault-normal data ( $k_H$ ),  $k_H$  ranges from  $1.51 \times 10^{-20}$  m<sup>2</sup> (IB07b; Fig. 2) to  $2.81 \times 10^{-18}$  m<sup>2</sup>  
107 (IB13a; Fig. 2);  $k_V$  ranges from  $6.54 \times 10^{-19}$  m<sup>2</sup> (IB07a; Fig. 2) to  $2.97 \times 10^{-17}$  m<sup>2</sup> (IB13a; Fig. 2).  
108 The permeability anisotropy ratio ( $k_V/k_H$ ) at 90 MPa effective pressure ranges from 11 to 43,  
109 with the maximum anisotropy in the lower-strain zone.

110 The studied basaltic host rocks are generally low permeability, within the range of  $10^{-20}$   
111 to  $10^{-19}$  m<sup>2</sup>, with the exception of the compound lava unit sample (L01; Fig. 2). The two sample  
112 suites (aphyric basalt lava unit and aphyric to plagioclasephyric basalt dyke) show a varied  
113 evolution pathway from host rock to evolved fault rock (Fig. 2). In the lava sample suite,  
114 permeability initially increases by about two orders of magnitude (from host to crackle breccia),  
115 but then decreases by a comparable amount into the higher-strain mosaic breccias. By contrast

116 the dyke sample suite shows an initial decrease in permeability from the host rock into the low  
117 strain fault rocks, followed by a near reciprocal increase toward the fault core. That permeability  
118 increase continues in the dyke suite into the fault core chaotic breccia, which records the highest  
119 permeabilities of this study (Fig. 2). A permeability increase is also recorded from the lava unit  
120 mosaic breccia (IB07) into the PSS cataclasite samples (IB13) (Fig. 2). Overall the sample suites  
121 show lower permeability in low strain zones, and higher permeability in high strain zones.

## 122 **FAULT ROCK ASSEMBLAGES**

123         Microstructural characterization of the host and fault rock assemblages is important as it  
124 gives insights into the controls of the static permeability laboratory measurements. Furthermore  
125 it gives a qualitative indication of the likely evolution in syn-faulting dynamic permeability with  
126 increasing deformation.

127         Sample suite host rocks are generally fine crystalline basalt, dominated by plagioclase  
128 and pyroxene, and display very minor mineral alteration to clays (Fig. 3A). This clay  
129 development appears to be authigenic, occurring along microfractures and crystal boundaries.  
130 Longer and wider fractures, where present, are typically clay-lined, and no zeolite or calcite  
131 mineralization is observed (Fig. 3A).

132         Low strain (<1m displacement) fault rocks (Fig. 3B) show increased alteration relative to  
133 the host, with discrete zones of clay minerals developed immediately adjacent to - and parallel  
134 with - fractures and veins (Fig. 3B). In samples L03 and IB07, zeolite veins are clay-lined and  
135 poorly connected in the section plane, whereas in samples S02 and L04, zeolite veins are  
136 interconnected. Blue-stained zeolite veins in thin section (Fig. 3B-C) indicate that these veins  
137 remain porous.

138 High strain (fault core) rocks that have accommodated m-scale displacements or greater  
139 (Fig. 3C) show intense zeolite and calcite veining that forms a connected network. Authigenic  
140 clays developed during host alteration appear to be absent in the crystalline groundmass, with  
141 zeolite fill in their place. PSS cataclasite samples that have accommodated ~30 m displacement  
142 (Fig. 3D) comprise chaotic, generally matrix-supported basalt, zeolite and calcite clasts set in a  
143 cataclasite matrix formed of the same components. Established vein networks are cut by, and  
144 incorporated into, the cataclasites.

145 Thin sections of measured samples show a strong correlation between clay development,  
146 section plane vein connectivity, and static permeability results. Where low strain fault rocks  
147 display poor zeolite-vein connectivity, permeability is higher than for samples with segmented  
148 veins. In the most permeable, high strain zones, clays are absent or dissected by zeolite/calcite  
149 (veins or continuous clasts of veins).

## 150 **IMPLICATIONS FOR PERMEABILITY STRUCTURE EVOLUTION**

151 The measured experimental static permeabilities when combined with field- and  
152 microstructural-characterization of the fault rocks show that faults in basalt generally develop  
153 through stages of low-strain, lower-permeability assemblages, to high-strain, higher permeability  
154 assemblages. This contrasts with most clastic-hosted fault zone models, where high strain fault  
155 cores are generally thought to exhibit lower permeabilities due to grain comminution effects (e.g.  
156 Caine et al., 1996). Microstructural evidence here indicates that the evolution of static  
157 permeability in basalt-hosted faults relates to the interplay between clay sealing versus zeolite  
158 vein connectivity, and cataclasis and vein dissection. The presence of pervasive mineral vein  
159 networks and authigenic clays within fault zones also indicate that there was significant transient  
160 permeability development during rock fracture episodes (i.e., dynamic permeability).

161 Although the host rocks from the sample suites are low-porosity fine crystalline basalts,  
162 microfractures related to cooling and/or distributed strain demonstrably facilitated transient, low  
163 fluid-flux, as is evidenced by the occurrence of minor alteration to clays. Depending on fluid  
164 chemistry (i.e., CO<sub>2</sub> concentration), pH and temperature, alteration of the basaltic mineralogy to  
165 clays within the study depth range (i.e., 0–3 km) can occur in a matter of years (Gysi and  
166 Stefánsson, 2008), i.e., at a rate comparable to aseismic fault creep. During initial meso- to  
167 macro-scale rock fracturing, fluid flow was increased locally, leading to the precipitation of  
168 zeolite and calcite as veins. In these low strain fault rocks, veins and fractures may remain  
169 locally statically permeable, but are lined by low-permeability clays and are poorly-  
170 interconnected (Fig. 3B). The development of clays acts to decrease permeability relative to the  
171 host rocks (Figs. 3A, B, 4). Such lowered permeabilities could help promote pore fluid trapping,  
172 ultimately resulting in pressure elevation and hydrofracture.

173 As fault displacement accumulates, the zeolite/calcite veins link to form through-going,  
174 transient high permeability pathways. Zeolite veins retain porosity following crystal growth (Fig.  
175 3B,C), maintaining high permeability after faulting. If these veins are interconnected, fault rock  
176 static permeability will remain high; if they are not connected, static permeability will be low  
177 (e.g., Figures 2, 3).

178 Larger displacement (>1 m) fault core samples principally comprise interconnected  
179 zeolite-calcite mineral-fills, with minor clay content only (Fig. 3C); hence static permeability is  
180 high. Further slip leads to static permeability reduction in the fault core through cataclasis, clay  
181 gouge development and dismemberment of existing zeolite/calcite veins. Nevertheless, the static  
182 permeability of the PSS (Figs. 2, 3D) remains over an order of magnitude higher (both  $k_V$  and  
183  $k_H$ ) compared to low strain fault rocks, despite fragmentation of the relatively high-permeability



184 veins, and development of a fine-grained matrix (cataclasite and/or gouge). Inspection of hand  
185 specimens suggests that this could be due to out of section-plane connectivity of permeable vein  
186 fragments (Fig. 3D).

187         The high-permeability, high strain zone, low-permeability low strain zone model  
188 presented here will promote lateral compartmentalization, and along-fault fluid migration.  
189 However, since the low strain zone forms a barrier to flow, fluids will only be able to migrate  
190 from and to relatively high permeability horizons (e.g., lava unit vesicular flow tops), bypassing  
191 the bulk of the lava flow stratigraphy via an ‘insulated’ fault core.

## 192 **ACKNOWLEDGMENTS**

193         This study was funded by Statoil U.K. Ltd. and the SINDRI Consortium. The authors  
194 thank D. Ellis, J. Imber, P. Cowie and three anonymous reviewers for constructive  
195 discussions and comments on earlier versions of this manuscript.

## 196 **REFERENCES CITED**

- 197 Armitage, P.A., Faulkner, D.R., Worden, R.H., Aplin, A.C., Butcher, A.R., and Iliffe, J., 2011,  
198 Experimental measurement of, and controls on, permeability and permeability anisotropy of  
199 caprocks from the CO<sub>2</sub> storage project at the Krechba Field, Algeria: *Journal of Geophysical*  
200 *Research*, v. 116, B12208, doi:10.1029/2011JB008385.
- 201 Brace, W.F., Walsh, J.B., and Frangos, W.T., 1968, Permeability of granite under high pressure:  
202 *Journal of Geophysical Research*, v. 73, p. 2225–2236, doi:10.1029/JB073i006p02225.
- 203 Caine, J.S., and Forster, C.B., 1999, Fault zone architecture and fluid flow: Insights from field  
204 data and numerical modeling, *in* Haneberg W.C., et al., eds., *Faults and Subsurface Flow in*  
205 *Shallow Crust: American Geophysical Monograph* 113, p. 101–127.

- 206 Caine, J.S., Evans, J.P., and Forster, C.B., 1996, Fault zone architecture and permeability  
207 structure: *Geology*, v. 24, p. 1025–1028, doi:10.1130/0091-  
208 7613(1996)024<1025:FZAAPS>2.3.CO;2.
- 209 Evans, J.P., Forster, C.B., and Goddard, J.V., 1997, Permeability of fault-related rocks, and  
210 implications for hydraulic structure of fault zones: *Journal of Structural Geology*, v. 19, p.  
211 1393-1404, doi: 10.1016/S0191-8141(97)00057-6
- 212 Ellis, D., Passey, S.R., Jolley, D.W., and Bell, B.R., 2009. Transfer zones: The application of  
213 new geological information from the Faroe Islands applied to the offshore exploration of  
214 intra basalt and sub-basalt strata, *in* Varming, T., and Ziska, H., eds., *Proceedings of the 2<sup>nd</sup>*  
215 *Faroe Islands Exploration Conference: Annales Societatis Scientiarum Færoensis,*  
216 *Supplementum*, v. 50, p. 174–204.
- 217 Faulkner, D.R., and Rutter, E., 2001, Can the maintenance of overpressured fluids in large strike-  
218 slip fault zones explain their apparent weakness: *Geology*, v. 29, p. 503–506,  
219 doi:10.1130/0091-7613(2001)029<0503:CTMOOF>2.0.CO;2.
- 220 Gislason, S.R., Wolff-Boenisch, D., Stefánsson, A., Oelkers, E.H., Gunnlaugsson, E.,  
221 Sigurdardottir, H., Sigfusson, B., Broecker, W.S., Matter, J.M., Stute, M., Axelsson, G., and  
222 Fridriksson, T., 2010, Mineral sequestration of carbon dioxide in basalt: A pre-injection  
223 overview of the CarbFix project: *International Journal of Greenhouse Gas Control*, v. 4,  
224 p. 537–545, doi:10.1016/j.ijggc.2009.11.013.
- 225 Gysi, A.P., and Stefánsson, A., 2008, Numerical modeling of CO<sub>2</sub>-water-basalt interaction:  
226 *Mineralogical Magazine*, v. 72, p. 55–59, doi:10.1180/minmag.2008.072.1.55.
- 227 Hawkins, D.G., 2004, No exit: thinking about leakage from geologic carbon storage sites:  
228 *Energy*, v. 29, p. 1571–1578, doi:10.1016/j.energy.2004.03.059.

- 229 Moy, D.J., and Imber, J., 2009, A critical analysis of the structure and tectonic significance of  
230 rift-oblique lineaments ('transfer zones') in the Mesozoic–Cenozoic succession of the  
231 Faroe–Shetland Basin, NE Atlantic margin: *Journal of the Geological Society*, v. 166,  
232 p. 831–844, doi:10.1144/0016-76492009-010.
- 233 Oelkers, E.H., and Cole, D.R., 2008, Carbon dioxide sequestration. A solution to a global  
234 problem: *Elements*, v. 4, p. 305–310, doi:10.2113/gselements.4.5.305.
- 235 Passey, S.R., and Jolley, D.W., 2009, A revised lithostratigraphic nomenclature for the  
236 Palaeogene Faroe Islands Basalt Group, NE Atlantic Ocean: *Earth and Environmental*  
237 *Science Transactions of the Royal Society of Edinburgh*, v. 99, p. 127–158,  
238 doi:10.1017/S1755691009008044.
- 239 Schutter, S.R., 2003, Hydrocarbon occurrence and exploration in and around igneous rocks, *in*  
240 Petford, N., and McCaffrey, K.J.W., eds., *Hydrocarbons in Crystalline Rocks: Geological*  
241 *Society, London, Special Publications 214*, p. 7–33.
- 242 Walker, R.J., Holdsworth, R.E., Imber, J., and Ellis, D., 2011a, Onshore evidence for progressive  
243 changes in rifting directions during continental break-up in the NE Atlantic: *Journal of the*  
244 *Geological Society*, v. 168, p. 27–48, doi:10.1144/0016-76492010-021.
- 245 Walker, R.J., Holdsworth, R.E., Imber, J., and Ellis, D., 2011b, The development of cavities and  
246 clastic infills along fault-related fractures in Tertiary basalts on the NE Atlantic Margin:  
247 *Journal of Structural Geology*, v. 33, p. 92–106, doi:10.1016/j.jsg.2010.12.001.
- 248 Walker, R.J., Holdsworth, R.E., Imber, J., and Ellis, D., 2012, Faults, fault rocks and fractures in  
249 flood basalt provinces: A case study from the Faroe Islands, NE Atlantic Margin: *Geological*  
250 *Society of America Bulletin*, doi:10.1130/B30512.1 (in press).

251 Woodcock, N.H., Omma, J.E., and Dickson, J.A.D., 2006, Chaotic breccia along the Dent Fault,  
252 NW England: Implosion or collapse of a fault void?: Journal of the Geological Society,  
253 v. 163, p. 431–446, doi:10.1144/0016-764905-067.

#### 254 **FIGURE CAPTIONS**

255 Figure 1. A: Overview of a dip slip normal fault in a columnar-jointed basalt unit (after Walker  
256 et al., 2012), showing idealized strain distribution. Map shows the location of the Faroe Islands  
257 and North Atlantic Igneous Province (NAIP). B: Low strain zone crackle and mosaic type fault  
258 breccias that accommodate mm- to cm-scale displacements. C: High strain (fault core)  
259 mineralized mosaic and chaotic breccias that accommodate about 5 m net slip. D: Principal slip  
260 zone chaotic breccia and cataclasites that accommodate >10 m displacement. Breccia styles  
261 defined following Woodcock et al. (2006).

262 Figure 2. Measured permeability data for host rock and fault rock assemblages at effective  
263 pressures ranging from 10 to 90 MPa (static fluid pressure of 10 MPa). Fault-parallel ( $k_V$ ) and  
264 fault-normal ( $k_H$ ) values are shown for anisotropic samples (IB07 and IB13). Host rock and  
265 chaotic breccias do not exhibit a clear fabric:  $k_V$  and  $k_H$  values are assumed equal within the  
266 experimental uncertainty. Within the sub-100 MPa confining pressure range, the high  
267 permeability of the dyke fault core sample (L05) is at the limits of the TPD technique using our  
268 experimental set-up; successful analysis at higher effective pressures (110–190 MPa; *Appendix*  
269 *2*), and down-pressure extrapolation indicate that fault core permeability ranges from  $\sim 2.5 \times 10^{-15}$   
270  $\text{m}^2$  at 10 MPa, to  $1.44 \times 10^{-16} \text{m}^2$  at 90 MPa.

271 Figure 3. Plane polarized light photo-micrographs of host rock and fault rock assemblages  
272 representative of samples used for experimental permeability measurement (i.e., Fig. 2). All  
273 samples were prepared using blue-stained resin to show porosity. See text for description and

274 discussion. A: Host rocks; B: Fault damage crackle (left) and mosaic (right) breccias; C: Fault  
275 core chaotic breccia; D: Principal slip zone comprising chaotic breccia and cataclasite and/or  
276 gouge. Disp.: displacement.

277 Figure 4. Summary model for the evolution of fault-parallel and fault-normal permeability, based  
278 on experimental data combined with microstructural characterization of fault zone assemblages.

279 <sup>1</sup>GSA Data Repository item 2012xxx, Appendix 1: Location maps for the study fault zones,

280 Faroe Islands, N. Atlantic European continental margin; Appendix 2: Experimental method

281 description, including table of results and graphs for all data, is available online at

282 [www.geosociety.org/pubs/ft2012.htm](http://www.geosociety.org/pubs/ft2012.htm), or on request from [editing@geosociety.org](mailto:editing@geosociety.org) or Documents

283 Secretary, GSA, P.O. Box 9140, Boulder, CO 80301, USA.

Figure 1  
w: 118 mm  
h: 72.2 mm

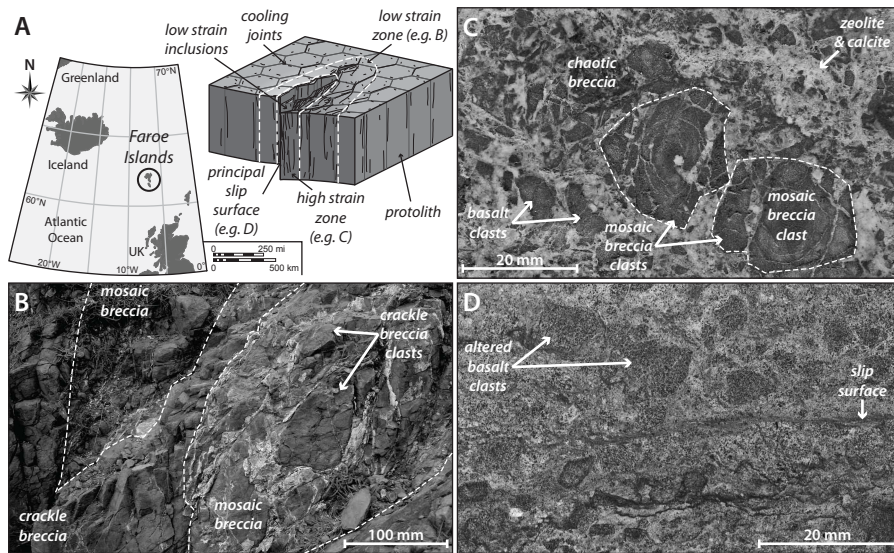


Figure 2  
w: 122.9 mm  
h: 63.5 mm  
(2 column width)

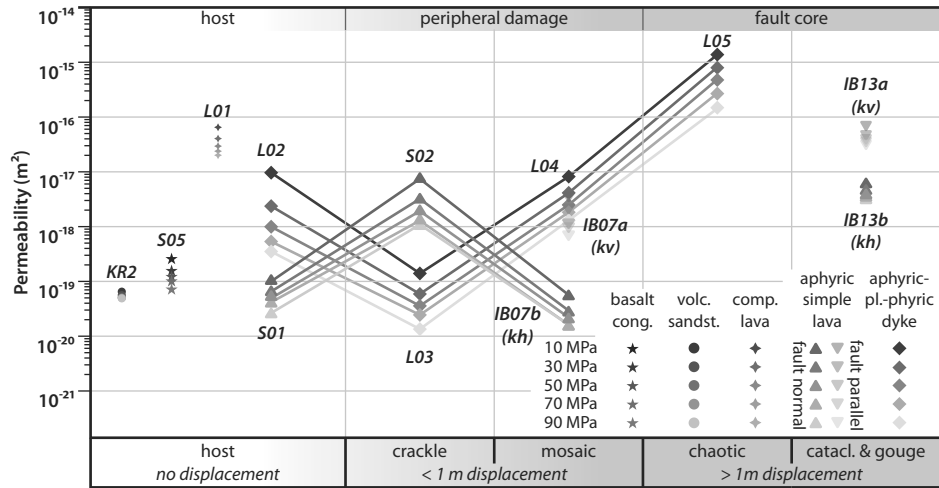


Figure 3  
w: 111.9 mm  
h: 222.5 mm  
(2 column; full page depth)

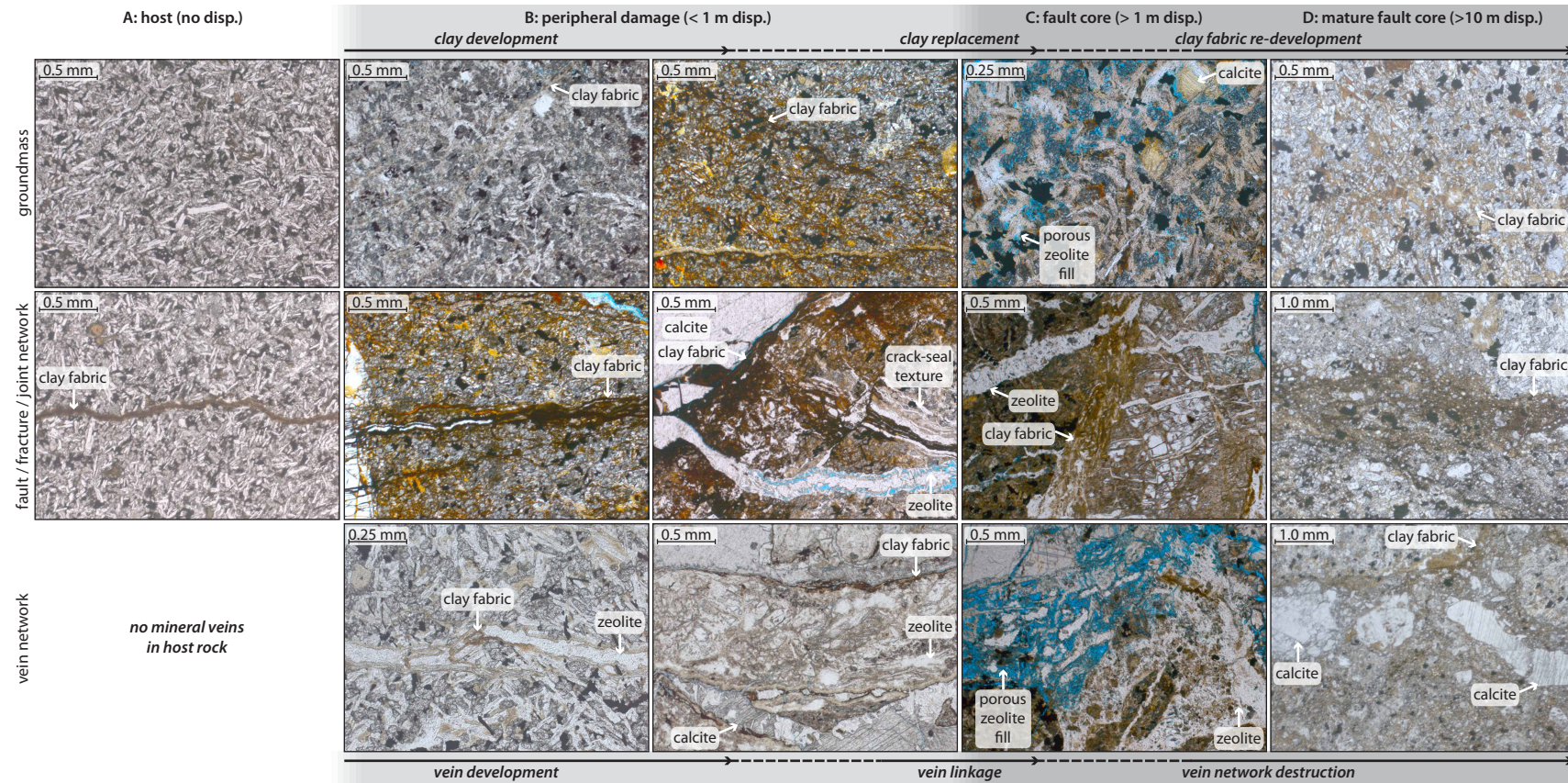




Figure 4  
w: 118 mm  
h: 70 mm  
(2 column width)

